JACS Au
AN OPEN ACCESS JOURNAL OF THE AMERICAN CHEMICAL SOCIETY

pubs.acs.org/jacsau

Article

Quantification of Active Site Density and Turnover Frequency: From Single-Atom Metal to Nanoparticle Electrocatalysts

Geunsu Bae,[○] Haesol Kim,[○] Hansol Choi, Pyeonghwa Jeong, Dong Hyun Kim, Han Chang Kwon, Kug-Seung Lee, Minkee Choi, Hyung-Suk Oh, Frédéric Jaouen,* and Chang Hyuck Choi*

Cite This: *JACS Au* 2021, 1, 586–597

Read Online

ACCESS | Metrics & More | Article Recommendations | Supporting Information

ABSTRACT: Single-atom catalysts (SACs) featuring atomically dispersed metal cations covalently embedded in a carbon matrix show significant potential to achieve high catalytic performance in various electrocatalytic reactions. Although considerable advances have been achieved in their syntheses and electrochemical applications, further development and fundamental understanding are limited by a lack of strategies that can allow the quantitative analyses of their intrinsic catalytic characteristics, that is, active site density (SD) and turnover frequency (TOF). Here we show an *in situ* SD quantification method using a cyanide anion as a probe molecule. The decrease in cyanide concentration triggered by irreversible adsorption on metal-based active sites of a model Fe−N−C catalyst is precisely measured by spectrophotometry, and it is correlated to the relative decrease in electrocatalytic activity in the model reaction of oxygen reduction reaction. The linear correlation verifies the surface-sensitive and metal-specific adsorption of cyanide on Fe−N_x sites, based on which the values of SD and TOF can be determined. Notably, this analytical strategy shows versatile applicability to a series of transition/noble metal SACs and Pt nanoparticles in a broad pH range (1−13). The SD and TOF quantification can afford an improved understanding of the structure−activity relationship for a broad range of electrocatalysts, in particular, the SACs, for which no general electrochemical method to determine the intrinsic catalytic characteristics is available.

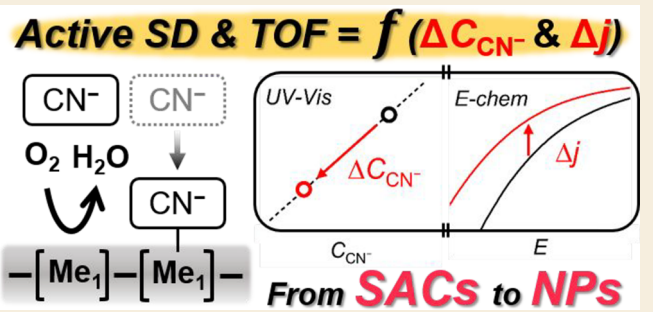

KEYWORDS: *Single-atom catalysts, Fe−N−C catalysts, active site density, turnover frequency, oxygen reduction reaction*

INTRODUCTION

Heterogeneous catalysts are of paramount importance to the world economy and the sustainable development of our society,[1,2] from chemical manufacturing to energy-related applications and environmental remediation. The overall apparent activity of a catalyst in a reaction can be expressed as a mathematical product of the active site density (SD) and turnover frequency (TOF). TOF, which is defined as the number of chemical conversions of reactant molecules per catalytic site and per unit time, is a key descriptor of the intrinsic activity of the catalytic site.[3] TOF is practically estimated by the combined input of the overall catalytic reaction rate (RR) of a catalyst and its SD (i.e., TOF = RR/SD). The availability of methods to deconvolute the apparent activity of a catalyst into its TOF and SD is important not only for fundamental understanding but also for guiding the rational development of novel catalysts,[4] as an increase in TOF or SD has different implications in the scientific rationale, experimental development of the next-generation catalytic materials, and their implementation in devices.

Chemisorption, titration, and other methods (e.g., X-ray diffraction line broadening analysis, small-angle X-ray scattering, etc.) have been employed to measure the SD values of heterogeneous catalysts in thermochemical reactions.[5−8] Among these methods, chemisorption under gas-phase conditions is generally used to determine the SD of a catalytic material.[9] However, in the field of electrocatalysis, the estimation of SD depends on the measurement of the electric charge exchanged during the interaction of the site-specific adsorbates with the catalytic surface immersed in an electrolyte. Since the adsorption/desorption events can be affected by the electrochemical potential and experimental conditions, the measurement of the SD values of electrocatalysts under the same conditions as those during the intended electrochemical reaction can prevent (or minimize) systemic errors. For example, the number of active sites probed in the gas phase would exceed that measured in the liquid phase for porous catalysts, whose active sites are located in the narrow pores that are not completely wetted by the electrolyte.[10] In addition, the

Received: February 19, 2021
Published: April 13, 2021

https://doi.org/10.1021/jacsau.1c00074
JACS Au 2021, 1, 586–597

surface properties of the catalysts can be altered under electrochemical conditions compared to those under the gas-phase conditions (e.g., because of contact with the liquid electrolyte and ionomer/binder, the reactant gas dissolved in the electrolyte, and the electrochemical potential applied). Consequently, the SD value measured at the gas/solid interface may not be directly applicable to the electrocatalysts experiencing a different environment of (gas/)liquid/solid interface during electrocatalysis. Hence, the concept of electrochemical active surface area (ECSA) has been introduced, which refers to the SD (or surface area) measured electrochemically, implying that the probed sites are both electrically and electrolytically connected. For the metallic surfaces of noble metals, the ECSA values are typically determined by measuring the electric charge during cyclic voltammetry (CV), which results from the underpotential deposition (UPD) of either hydrogen (H_{UPD}) or metal ions (e.g., Cu_{UPD})[11−13] or from the electrochemical oxidation of strongly adsorbed species (e.g., CO-stripping).[14−16] However, these *in situ* electrochemical methods are restricted to the metallic surfaces of platinum-group metals (PGMs) and are not applicable to a multitude of other catalysts that do not adsorb H or CO under such conditions. In particular, the measurement of SD under electrochemical conditions remains challenging for the recent promising single-atom catalysts (SACs) featuring atomically dispersed active metal sites, which have completely different characteristics from bulk metal catalysts.[17]

The Me−N−C catalyst, one of the promising class of SACs comprising metal−N_x sites, has attracted significant attention for catalyzing various electrochemical reactions (e.g., oxygen reduction, hydrogen evolution, and carbon dioxide reduction reactions),[18−23] but shows no H and CO adsorption under ambient conditions, thereby limiting the quantification of SD in electrochemical environments. Although X-ray absorption spectroscopy (XAS) and ^{57}Fe or ^{119}Sn Mössbauer spectroscopy are powerful tools for identifying the Me−N_x moieties,[24−27] such techniques employing high-energy radiation probe the entire volume and are not surface specific. The measurement of the electric charge based on the redox transitions of the metal center can be an effective method to determine the SD of SACs,[28,29] but is applicable only when they contain a well-defined Me−N_x site (e.g., nonpyrolyzed macrocycles or molecular complexes on carbon) and is generally not reliable for Me−N−C, where the redox feature is broad and weak because of the covalently integrated Me−N_x sites in the N-doped carbon matrix.

For studies on Me−N−C, only two methods for SD quantification employing molecular probes have been established.[30,31] The first method is low-temperature CO cryo chemisorption at 193 K.[30] The weakness of this method includes: (1) a possible overestimation of SD since all gas-phase accessible sites can be probed (in particular for Me−N−C with high microporosity) and (2) its limitation to the quantification of Me−N_x sites with a sufficiently strong binding of CO* (i.e., Fe and Mn).[32] In addition, a thermal pretreatment up to 873 K is necessary to completely remove the preadsorbed O_2 on Me−N_x sites before CO adsorption. This cleaning treatment can lead to unexpected modifications in the surface chemistry, possibly changing its SD and/or TOF for a particular reaction.[33] The second method is nitrite (NO_2^-)-stripping voltammetry.[31] This is an *in situ* electrochemical method performed at a specific pH (pH 5.2; 0.5 M acetate buffer), which quantifies the electric charge corresponding to the reduction of the nitrosyl ligand on the Fe−N_x sites. The conversion of this electric charge into a SD value is performed by hypothesizing that the electrochemical reduction of the Fe nitrosyl complex (generated by a well-known chemical reaction between NO_2^- and protons) is selective and complete toward ammonia (five-electron reduction).[34,35] The NO_2^--stripping method has advantages compared to the CO chemisorption as it is an *in situ* method. However, the application of this method for evaluating the SD of the SACs other than Fe−N−C or in a broad pH range is challenging owing to the unknown number of electrons transferred during the nitrosyl reduction under different conditions. In addition to the complete five-electron reduction product, ammonia, several other products of the nitrosyl reduction reaction can be expected, for example, hydroxylamine, nitrous oxide, and nitrogen, depending on the catalytic material and electrolyte pH.[36−38] Recently, a non-negligible deviation between the SD values, measured by CO chemisorption and NO_2^--stripping voltammetry on four benchmark Fe−N−C catalysts, has also been reported.[39]

Herein, a versatile *in situ* method for SD quantification is proposed by employing a cyanide anion probe. Although cyanide has been reported to poison Fe−N−C catalysts in prior studies,[40,41] it has not been used to quantify their SDs owing to its competitive adsorption with O_2.[42] Here, a new strategy to determine the SD of Fe−N−C is developed based on the combination of (1) partial cyanide poisoning of Fe^{3+}-N_x surface sites free of O_2 ligand and (2) the ensuing relative deactivation in the model reaction of oxygen reduction reaction (ORR). The decrease in cyanide concentration due to its adsorption on Fe^{3+}−N_x is quantified using ultraviolet−visible (UV−vis) spectrophotometry, as a photoactive compound is formed via a cascade reaction between cyanide and *p*-nitrobenzaldehyde, which is further correlated to the relative decay in ORR activity. This SD quantification protocol is highly surface sensitive and metal specific, allowing the determination of SD and TOF of Fe−N−C. Notably, this analytical method is applicable under various electrochemical conditions ranging from acidic to alkaline environments and shows a broad material scope ranging from Me−N−C (Me = Mn, Co, and Ni) to Pt-SAC comprising atomically dispersed Pt in sulfur-doped carbon as well as conventional Pt metallic nanoparticles supported on carbon.

RESULTS AND DISCUSSION

A model Fe−N−C catalyst (labeled '$Fe_{0.5}$NC'),[43,44] comprising only atomically dispersed Fe−N_x moieties without metallic or oxide/carbide Fe clusters, was employed to develop the *in situ* SD quantification method (see details for the synthetic procedure in the Experimental Section). The Fe−N−C catalyst was chosen as a model substance primarily because previous CO chemisorption and NO_2^--stripping methods for SD estimation have been developed with Fe−N−C catalyst(s), allowing us to directly compare the SD values measured by multiple methods. The detailed physicochemical characterization results of $Fe_{0.5}$NC can be found in Supplementary Note 1 (Figure S1 and Tables S1 and S2).

Despite the reported poisoning effects of cyanide on the ORR activity of Fe−N−C catalysts,[40,41] SD quantification with this probe anion has not yet been successfully established. This is primarily because cyanide weakly adsorbs on the Fe−N_x sites, thus showing competitive adsorption with O_2.[42] The

https://doi.org/10.1021/jacsau.1c00074
JACS Au 2021, 1, 586−597

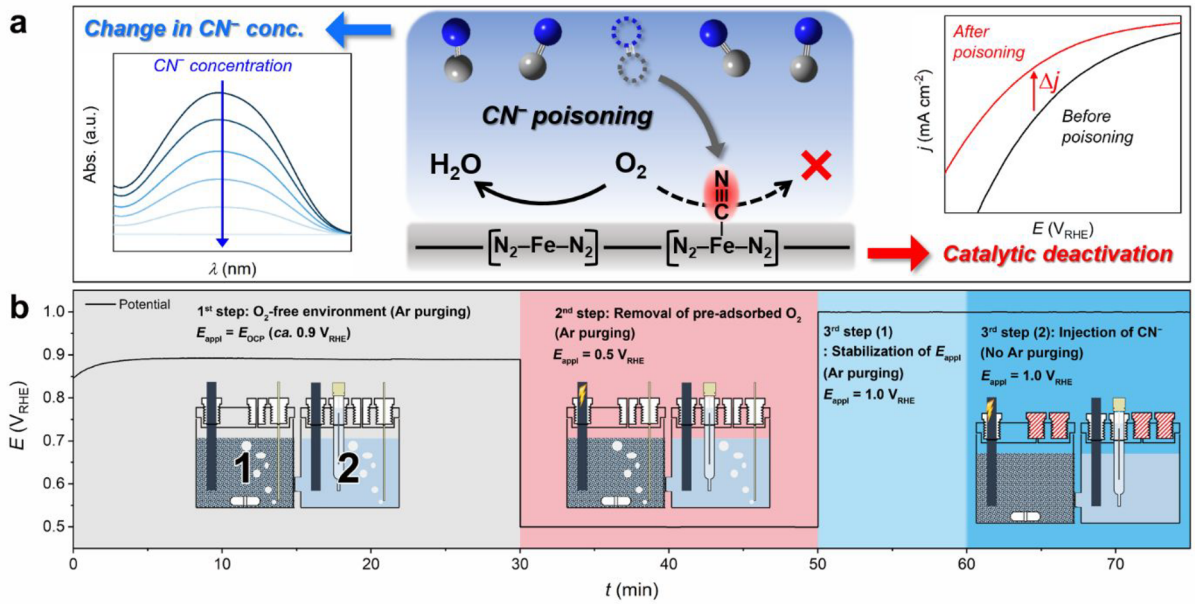

Figure 1. Scheme of *in situ* SD quantification protocol using a cyanide probe. (a) *In situ* SD quantification procedure depends on the combined measurement of the decrease in the cyanide concentration (left-hand-side inset in (a)) due to its adsorption on the metal-based active sites (central scheme in (a); blue = N, gray = C) and irreversible decrease in ORR activity after cyanide poisoning (right-hand-side inset in (a)). (b) *In situ* cyanide poisoning protocol comprises three steps: (1) removal of predissolved O_2 in the electrolyte by Ar purging, (2) electrochemical removal of preadsorbed O_2 on the catalyst, and (3) cyanide poisoning of the catalyst under the controlled electrochemical potential of the working electrode.

relatively weak adsorption of cyanide on Fe−N_x sites compared to O_2 is supported by the recovery of most of the initial ORR activity of Fe−N−C after simple rinsing with water.[42,45] When the cyanide concentration in the electrolyte is significantly higher than that of O_2 (ca. 1−1.5 mM O_2 in aqueous electrolytes at room temperature; RT), the equilibrium between cyanide and O_2 occupation of Fe−N_x sites is displaced toward the former owing to Le Chatelier's effect.[42]

Hence, a SD quantification protocol based on cyanide adsorption on Fe−N_x sites demands some prerequisites. First, the electrochemical environments and active sites must be free of O_2, such that cyanide can potentially bind to most of the surface active sites. Second, cyanide poisoning must be irreversible, such that the ORR activity of the cyanide-poisoned sample can be measured in a cyanide-free O_2-saturated electrolyte. To quantify the amount of cyanide adsorbed (and thus the number of surface sites occupied by cyanide, assuming a 1:1 ratio) on Fe−N−C under specific conditions, the changes in the cyanide concentration in the electrolyte ($C_{CN^-}^{electrolyte}$) and the ORR activity before and after cyanide adsorption by $Fe_{0.5}$NC need to be quantified (Figure 1a). A highly sensitive spectrophotometric method was selected to achieve this goal. This method was based on the cascade chemical reaction of cyanide with *p*-nitrobenzaldehyde, followed by a reaction with tetrazolium blue to produce a photoactive diformazan compound (Figure S2).[46,47] The final product yielded maximum absorbance at ca. 520 nm in the UV−vis spectrum, and the absorbance was linearly proportional to the cyanide concentration in the UV−vis cuvette ($C_{CN^-}^{cuvette}$), which was 0−10 μM (Figure S3). The correlation between UV−vis absorption at 520 nm and cyanide concentration is sufficiently accurate to measure very low cyanide concentrations, providing a suitable analytical platform for detecting small changes in $C_{CN^-}^{electrolyte}$ before and after the cyanide poisoning of $Fe_{0.5}$NC.

Cyanide poisoning of $Fe_{0.5}$NC was carried out in a two-compartment H-type electrochemical cell (Figure 1b). Each compartment was initially filled with 0.1 M $HClO_4$ electrolyte, and a graphite-rod working electrode was placed in compartment 1, while the counter and reference electrodes were placed in compartment 2. The two compartments were separated using a Nafion membrane. The key reason for the separation was to prevent pollution by O_2 produced at the counter electrode during the electrochemical removal of O_2 in compartment 1. A known amount of $Fe_{0.5}$NC powder was dispersed only in working electrode compartment 1 and mechanically stirred to prevent its sedimentation during the entire poisoning protocol. Following the addition of $Fe_{0.5}$NC, the electrolyte was deaerated by Ar purging, while the working electrode was set at the open circuit potential (OCP), and all subsequent (electro)chemical treatments were conducted in an Ar-filled chamber to prevent undesirable O_2 dissolution in the electrolyte (first step). In the next step, preadsorbed O_2 on the Fe−N_x sites, which could not be simply removed by Ar purging, was electrochemically removed. This was performed under continuous Ar purging and mechanical stirring by applying a sufficiently low potential of 0.5 V_{RHE} to the working electrode (second step), to ensure that the preadsorbed O_2 was reduced to water when the catalyst particles collided with the working electrode through convective motion. Subsequently, an aliquot of deaerated cyanide aqueous solution was injected into both compartments (third step). The initial $C_{CN^-}^{electrolyte}$ was adjusted to 200 μM, resulting in an optimized balance between the irreversible poisoning of Fe−N_x sites and a significant decrease in cyanide concentration. The working electrode was polarized at 1.0 V_{RHE} (i.e., E_{third}) to ensure that the surface Fe−N_x sites were in the ferric state (Figure S4). The ferric state of Fe−N_x sites has a higher binding affinity to cyanide than the ferrous state, based on the studies on hemoproteins and Fe cyanide complexes.[48,49] After cyanide injection, Ar purging was stopped, and all compartments were closed to prevent any

https://doi.org/10.1021/jacsau.1c00074
JACS Au 2021, 1, 586−597

undesirable decrease in cyanide concentration via the release of HCN in the gas-phase (Figure S5).

The decrease in $C_{CN^-}^{electrolyte}$ due to cyanide adsorption by $Fe_{0.5}NC$ was then measured by UV−vis spectrophotometry. An aliquot of the electrolyte, which was collected after filtering the solution of compartment 1 from $Fe_{0.5}NC$, was diluted 20 times, and a fixed amount of *p*-nitrobenzaldehyde and tetrazolium blue was added (see Experimental Section). Control experiments without the addition of a catalyst in compartment 1 or with the addition of Fe-free N-doped carbon (NC) revealed a negligible decrease in $C_{CN^-}^{electrolyte}$ after the poisoning protocol (Figure 2a,b). On the other hand, the

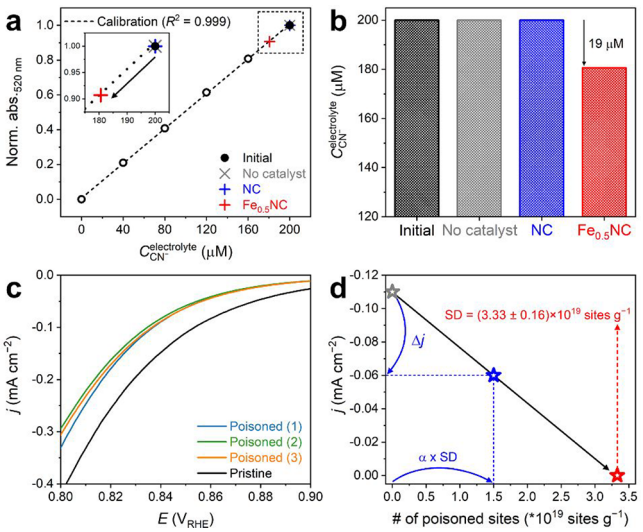

Figure 2. *In situ* SD quantification of $Fe_{0.5}NC$ using the cyanide probe method. (a) Determination of $C_{CN^-}^{electrolyte}$ using a UV−vis spectrophotometer at 520 nm before and after cyanide adsorption on $Fe_{0.5}NC$. Results obtained for the two control experiments, that is, without any catalyst (gray cross) and with NC in solution (blue cross), are also compared. Calibration values are indicated by open circles, and initial $C_{CN^-}^{electrolyte}$ is indicated by a filled circle. (b) Initial cyanide concentration (same for all three experiments) and cyanide concentration after the blank experiment without any catalyst or the cyanide poisoning of NC and $Fe_{0.5}NC$ in solution. (c) ORR activity of $Fe_{0.5}NC$ measured in O_2-saturated 0.1 M $HClO_4$ electrolyte before and after *in situ* SD quantification with cyanide poisoning. Three repeated experiments are presented. (d) Estimation of the SD value of $Fe_{0.5}NC$ (red star) by linear extrapolation to zero current of the line defined by the initial point (gray star; pristine $Fe_{0.5}NC$) and second point (blue star; cyanide-poisoned $Fe_{0.5}NC$). The *x* and *y* positions of each point are defined by the measured absolute amount of Fe−N_x sites poisoned and ORR activity after cyanide poisoning, respectively.

spectrophotometric data collected after the addition of $Fe_{0.5}NC$ showed that $C_{CN^-}^{electrolyte}$ decreased from 200 to 181 μM after the cyanide poisoning of $Fe_{0.5}NC$, indicating that the surface Fe−N_x moieties adsorbed cyanide ions. The poisoned $Fe_{0.5}NC$ powder that was collected after filtration and water rinsing showed a current density (*j*) of −0.060 ± 0.003 mA cm^{-2} at 0.85 V_{RHE} (Figure 2c), which was significantly lower than that of pristine $Fe_{0.5}NC$ (j = −0.110 mA cm^{-2}). Cyanide was hardly detected in the rinsed water (Figure S6), which indicates the irreversible adsorption of cyanide on the Fe−N_x site during the poisoning protocol.

However, any O_2 contamination in the electrolyte during the protocol could interrupt the cyanide poisoning of $Fe_{0.5}NC$, likely due to the competitive adsorption of O_2 on Fe−N_x sites (Figure S7). It is of note that the ORR activity was measured by linear sweep voltammetry (LSV) in a restricted potential range of 0.70−1.05 V_{RHE} with a low scan rate of 1 mV s^{-1}, which afforded high reproducibility of the ORR polarization curves for the pristine and poisoned catalysts (Supplementary Note 2 and Figures S8 and S9).

Then, SD could be derived from the change in cyanide concentration ($\Delta C_{CN^-}^{electrolyte}$) and the relative decrease in ORR activity ($\Delta j/j_{pristine}$) obtained from the collected cyanide-poisoned $Fe_{0.5}NC$ powder. If it is assumed that the decrease in ORR activity is linear to the amount of adsorbed cyanide on the surface Fe−N_x moieties from zero to "SD" and the ORR activity reaches zero when all surface Fe−N_x sites are occupied by cyanide (Figure S10), their relationship can be expressed by the following equation:

$$\Delta j/j_{pristine} = (\alpha \times SD)/SD \quad (1)$$

where α is the fraction of poisoned sites to total sites (i.e., poisoned + nonpoisoned) of Fe−N_x species, and $j_{pristine}$ and Δj are the pristine catalytic activity and poisoning-induced activity decrease at a given potential, respectively. Then, SD can be expressed by the following equation:

$$SD\,[sites\ g^{-1}] = (\Delta C_{CN^-}^{electrolyte} \times V \times N_A/m_{cat})/(\Delta j/j_{pristine}) \quad (2)$$

where V is the electrolyte volume (40 mL), N_A is the Avogadro constant, and m_{cat} is the catalyst amount (30 mg).

However, eqs 1 and 2 are based on the linearity hypothesis (Figure S10). Hence, the above calculations are valid only when the cyanide poisoning on Fe−N_x sites occurs in a similar manner on all surface Fe−N_x sites. If there are two or more types of surface Fe−N_x sites on $Fe_{0.5}NC$ with different affinities for cyanide binding, the SD value estimated according to eq 2 will be erroneous (Supplementary Note 3). Considering this hypothesis using eqs 1 and 2, the estimated SD value was (3.33 ± 0.16) × 10^{19} sites g^{-1} for $Fe_{0.5}NC$ (Figure 2d). Based on the SD value and measured bulk metal content, the utilization factor (U) of $Fe_{0.5}NC$ can be calculated using eq 3, which represents the electrochemically accessible active metal sites to the total number of metal atoms in the material.

$$U\,[\%] = 100 \times m_{surf}/m_{bulk} = 100 \times SD/\left(\frac{\%_{Me}}{100} \times \frac{N_A}{M}\right) \quad (3)$$

where m is the metal content at the surface and bulk, $\%_{Me}$ is the weight percentage of the metal in the catalyst, and M is the atomic mass of the metal. Using eq 3 and the SD values obtained for three different repetitive experiments, U was determined to be 20−22% in $Fe_{0.5}NC$.

To verify whether these assumptions and the results obtained using this new method were reliable, the SD and U values were estimated with different extents of cyanide poisoning of $Fe_{0.5}NC$ (Figure 3). The first approach to modulate the extent of cyanide poisoning comprised the application of different potentials on the working electrode during the third step of the poisoning protocol (third step in Figure 1b). In comparison to the original protocol (E_{third} = 1.0 V_{RHE}), the results showed that cyanide adsorption on $Fe_{0.5}NC$ was mitigated when E_{third} decreased from 1.0 to 0.7 V_{RHE} (Figure 3a). The $\Delta C_{CN^-}^{electrolyte}$ of ca. 19 μM at 1.0 V_{RHE} decreased to ca. 14 μM at 0.7 V_{RHE}. *In situ* X-ray absorption near edge structure (XANES) measurements at different

https://doi.org/10.1021/jacsau.1c00074
JACS Au 2021, 1, 586−597

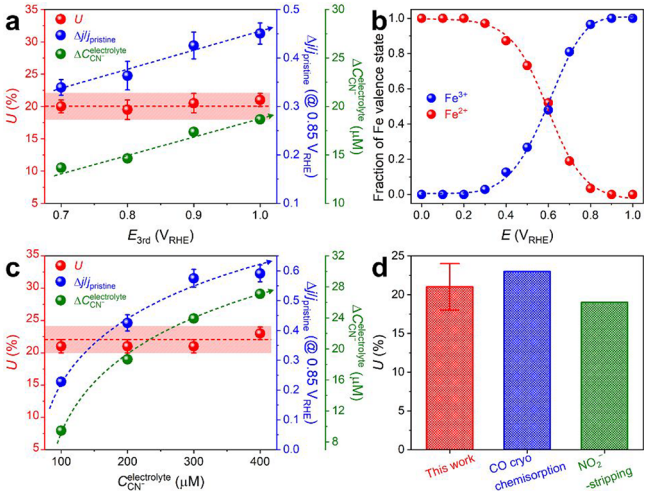

Figure 3. Determination of U values under various conditions of *in situ* SD quantification. (a) U, $\Delta j/j_{pristine}$, and $\Delta C_{CN^-}^{electrolyte}$ values estimated at different E_{third} values applied on the working electrode. (b) Fraction of ferric and ferrous ions of $Fe_{0.5}NC$ at various potentials, fitted from the Fe K-edge *in situ* XANES spectra (Figure S4b). (c) U, $\Delta j/j_{pristine}$, and $\Delta C_{CN^-}^{electrolyte}$ values estimated at different initial $C_{CN^-}^{electrolyte}$ values in the working electrode compartment. (d) Comparison of the U values of $Fe_{0.5}NC$ measured by the cyanide-poisoning *in situ* SD quantification, gas-phase CO chemisorption, and electrochemical NO_2^--stripping methods.[31,33]

potentials suggested that the decrease in $\Delta C_{CN^-}^{electrolyte}$ is attributed to a decrease in the population of ferric species with a higher binding affinity to cyanide than the ferrous species (Figures 3b and S4b).[48,49] However, with a decrease in $\Delta C_{CN^-}^{electrolyte}$, the ORR activity loss for $Fe_{0.5}NC$ also decreased simultaneously (Figure S11). This led to comparable SD ($(3.20 \pm 0.30) \times 10^{19}$ sites g^{-1}) and U ($20 \pm 2\%$) values, regardless of the applied E_{third} values (Figure 3a), because the proportional changes in $C_{CN^-}^{electrolyte}$ and $\Delta j/j_{pristine}$ canceled out in eq 2. In the second approach, the extent of cyanide poisoning was modified by varying the initial $C_{CN^-}^{electrolyte}$ values in compartment 1 from 100 to 400 μM (200 μM for the original protocol). The results showed that $\Delta C_{CN^-}^{electrolyte}$ increased from ca. 9 to 27 μM with an increase in the initial $C_{CN^-}^{electrolyte}$ (Figure 3c). Similar to the effects observed with the electrochemical potential modulation, $\Delta C_{CN^-}^{electrolyte}$ and $\Delta j/j_{pristine}$ changed proportionally (both increased when the initial $C_{CN^-}^{electrolyte}$ was increased; Figure S12), thereby resulting in similar values of SD ($(3.52 \pm 0.34) \times 10^{19}$ sites g^{-1}) and U ($22 \pm 2\%$) for the initial $C_{CN^-}^{electrolyte}$ values ranging from 100 to 400 μM (Figure 3c).

Therefore, the effects of the potential applied in the third step and initial cyanide concentration afforded almost identical SD ($(3.38 \pm 0.48) \times 10^{19}$ sites g^{-1}) and U ($21 \pm 3\%$) values, even though different amounts of cyanide were irreversibly adsorbed on $Fe_{0.5}NC$. This observation clearly supports the random cyanide poisoning on all surface Fe−N_x sites of $Fe_{0.5}NC$, verifying the validity of the assumptions in eqs 1 and 2 (Supplementary Note 3). Notably, the U values obtained by the present *in situ* cyanide poisoning method (21% on average) were slightly lower than those measured previously using the *ex situ* CO cryo chemisorption method (ca. 23%; Figure S13), but were slightly higher than those obtained by the modified *in situ* NO_2^--stripping method (ca. 19%; Figure S14) for an identically prepared catalyst (Figure 3d). It is of note that a different hypothesis for the final product of nitrosyl ligand reduction was employed for the NO_2^--stripping method. Together, these results imply that the cyanide probe in the liquid electrolyte can easily access the active sites, and this *in situ* protocol provides a new analytical platform for the accurate quantification of active Fe−N_x sites on Fe−N−C catalysts in acidic environments.

With the SD descriptor obtained by a combination of spectrophotometry and a decrease in catalytic activity, the TOF of $Fe_{0.5}NC$ in ORR could be calculated using the following equation:

$$J\,[Ag^{-1}] = (TOF \times SD \times F)/N_A \quad (4)$$

where J is the catalytic mass activity at a given potential and F is the Faraday constant. In an acidic medium, the TOF of $Fe_{0.5}NC$ was determined to be 0.40 ± 0.05 e site^{-1} s^{-1} at 0.80 V_{RHE} through control experiments performed with different E_{third} and $C_{CN^-}^{electrolyte}$ values, which showed small deviations in the TOF values. The TOF of $Fe_{0.5}NC$ was calculated using the SD value, which was obtained at 0.85 V_{RHE} owing to the non-negligible limitation of the current density by diffusion below 0.85 V_{RHE} (Figure S9). This TOF is slightly higher (but in the same order of magnitude) than that measured by CO chemisorption using an identically prepared and other Fe−N−C catalysts (0.15−0.18 e site^{-1} s^{-1}),[26,33] probably due to a possible overestimation in SD value measured at the gas-phase condition.

In addition to the determination of SD and TOF for the Fe−N−C catalyst, which can also be achieved by the previous CO chemisorption and NO_2^--stripping methods,[31,33] the general applicability of the cyanide protocol was investigated under various experimental conditions and on other electrocatalytic materials (Figure 4). First, to examine the applicability of the cyanide protocol in conditions other than the acidic electrolyte (pH 1), the SD of $Fe_{0.5}NC$ was measured in neutral (pH 7; 0.1 M phosphate buffer) and alkaline (pH 13; 0.1 M KOH) electrolytes. As the SD value (in this case, the number of Fe−N_x sites) is an inherent characteristic of the catalytic material, it was expected that if the cyanide protocol is applicable under neutral and alkaline conditions and no significant demetalation of Fe−N_x sites occurs in acidic pH (as suggested by slightly lower SDs than the gas-phase CO chemisorption), the SD of the $Fe_{0.5}NC$ catalyst measured at pH 7 and 13 should be similar to that measured at pH 1. In practice, $\Delta C_{CN^-}^{electrolyte}$ values in neutral and alkaline electrolytes (ca. 16 and 17 μM at pH 7 and 13, respectively; Figure S15) were similar (or slightly lower) to that measured in the acidic electrolyte (ca. 19 μM), resulting in comparable U values (19 $\pm$ 1%) regardless of the electrolyte pH (Figure 4a,f). This result indicated that the cyanide protocol could be applied to measure the SD of the Fe−N−C catalysts over a broad range of pH values. Although this does not provide additional information if the SD is pH-independent, it brings direct information regarding the TOFs of the Fe−N_x sites for ORR at different pH values.

Subsequently, the applicability of the cyanide protocol to quantify the SDs of the other SACs was examined. First, other Me−N−C catalysts (Me = Mn, Co, and Ni; labeled '$Me_{0.5}NC$') were prepared in a similar manner as $Fe_{0.5}NC$ by changing only the metal. Because these transition metals have similar atomic masses (i.e., 54.9−58.7 amu) and the carbonization of ZIF-8 as well as the formation of Me−N_x moieties occur during flash pyrolysis (i.e., increase in temperature from

https://doi.org/10.1021/jacsau.1c00074
JACS Au 2021, 1, 586−597

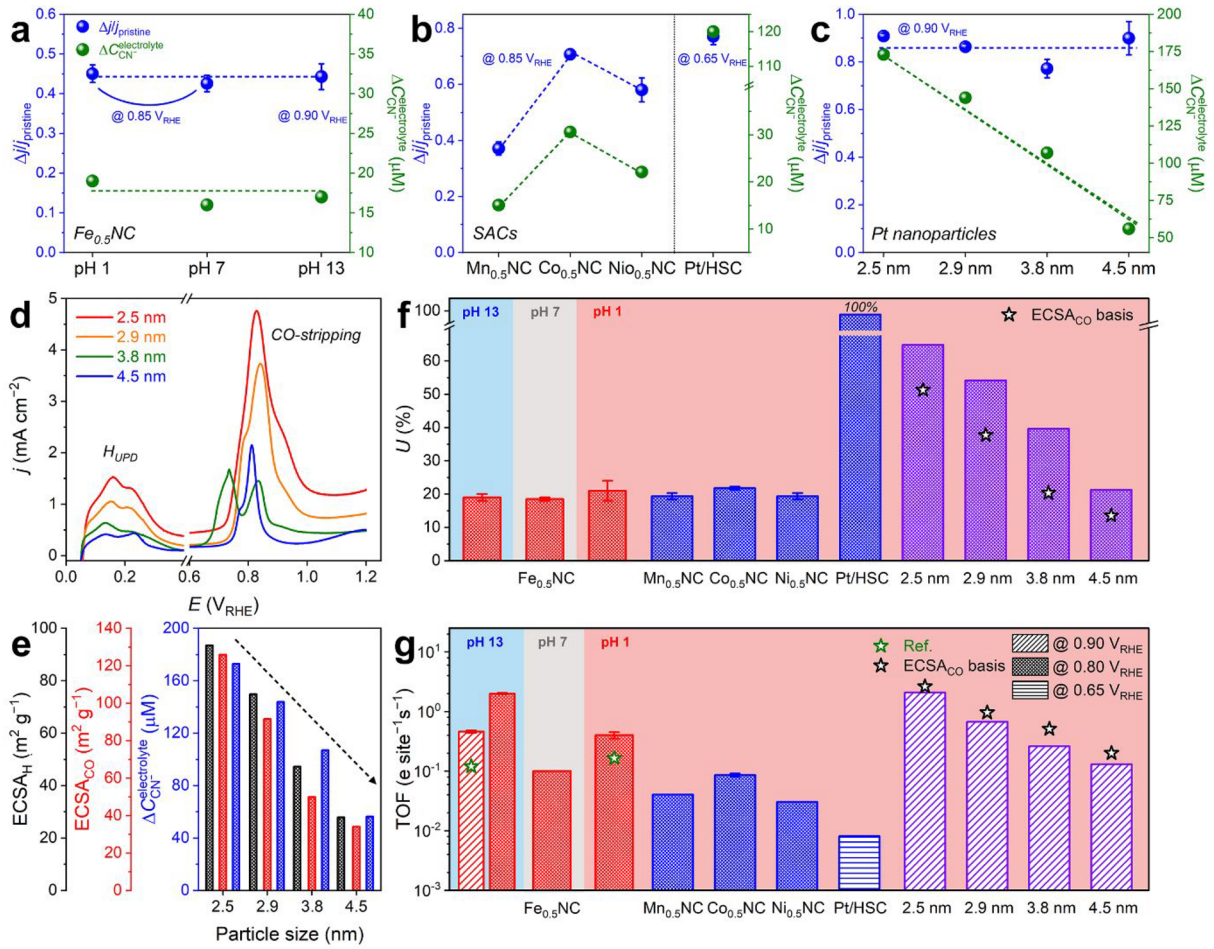

Figure 4. General applicability of cyanide-poisoning *in situ* SD quantification protocol. (a–c) $\Delta j/j_{pristine}$ and $\Delta C_{CN^-}^{electrolyte}$ values obtained after the *in situ* SD quantification of $Fe_{0.5}NC$ at various pH values (a), $Me_{0.5}NC$ (Me = Mn, Co, and Ni) and Pt/HSC (b), and Pt nanoparticles with different particle sizes (i.e., 2.5, 2.9, 3.8, and 4.5 nm) (c). (d) H_{UPD} and CO-stripping voltammograms of Pt nanoparticles. (e) Comparison between ECSA values, derived from H_{UPD} (black *y*-axis) and CO-stripping (red *y*-axis), and $\Delta C_{CN^-}^{electrolyte}$ (blue *y*-axis) for Pt nanoparticles with different particle sizes. (f,g) Summary of *U* (f) and TOF (g) values estimated by the *in situ* SD quantification of $Fe_{0.5}NC$ at various pH values and other control SACs and Pt nanoparticles at pH 1. The values reported in the literature (green star) or obtained by $ECSA_{CO}$ (black star) are also included for comparison.[26,33]

RT to 1323 K within a few seconds), it can be reasonably surmised that the physicochemical characteristics of the $Me_{0.5}NC$ catalysts are similar to those of $Fe_{0.5}NC$. In particular, metal content in the $Me_{0.5}NC$ catalysts was ca. 1.5 wt %, and most of the metal species were dispersed as $Me-N_x$ moieties as confirmed by XAS spectra (Figures S16–S18 and Table S1). This was consistent with identical physicochemical characteristics (except for the nature of the metal) for other series of $Me_{0.5}NC$ catalysts prepared via the same synthetic protocol and studied for CO_2RR and ORR to H_2O_2.[50,51]

In the SD quantification, the $\Delta C_{CN^-}^{electrolyte}$ values of $Mn_{0.5}NC$, $Co_{0.5}NC$, and $Ni_{0.5}NC$ were ca. 15, 31, and 22 μM, respectively (Figure S19). This difference (under identical conditions applied during the protocol) highlighted the different binding affinities of cyanide on $Me-N_x$ sites as a function of the metal characteristics.[48] However, the similar trends of $\Delta j/j_{pristine}$ values as those of $\Delta C_{CN^-}^{electrolyte}$ resulted in *U* values of 21 ± 2% for all $Me_{0.5}NC$ catalysts, which were comparable to that of $Fe_{0.5}NC$ (Figure 4b,f). These results indicated that the fraction of surface $Me-N_x$ species to total $Me-N_x$ species was similar for all catalysts in this series, which was reasonable based on similar active site structure and surface area of this series of materials.[50,51]

Thereafter, a catalyst featuring single-atom Pt sites was introduced, in which atomically dispersed Pt^{2+} species (5 wt % Pt content) were ligated by the thiophene/thiolate functionalities of S-doped carbon (Figure S20; named "Pt/HSC").[52,53] Unlike the unitary process of $Fe_{0.5}NC$ (and $Me_{0.5}NC$) synthesis, Pt/HSC was synthesized by the stabilization of isolated active Pt species ($Pt^{2+}-S_4$) via conventional wet impregnation on the prepared HSC support (see Experimental Section). This afforded the predominant presence of $Pt-S_4$ moieties at the HSC surface and expectedly complete utilization of Pt (i.e., U = ∼100%). Consequently, with this model catalyst, the accuracy of the cyanide protocol and its extension to SD quantification of PGM-based SACs, which have attracted significant attention owing to their unique electrocatalytic characteristics,[54−56] could be directly evaluated. The SD quantification results afforded $\Delta C_{CN^-}^{electrolyte}$ values of 10 and 120 μM for HSC and Pt/HSC, respectively (Figure S21). The difference (110 μM) indicated that $\Delta C_{CN^-}^{electrolyte}$ was induced by cyanide adsorption on the isolated $Pt-S_4$ moieties. Based on the decrease in the ORR activity following cyanide

https://doi.org/10.1021/jacsau.1c00074
JACS Au 2021, 1, 586–597

poisoning from −0.077 to −0.018 ± 0.002 mA cm^{-2} at 0.65 V_{RHE} (Figure S21), the $\Delta C_{CN^-}^{electrolyte}$ value of 110 μM corresponds to almost 100% utilization of Pt in Pt/HSC (Figure 4b,f).

After demonstrating the validity of the cyanide protocol for SD measurements of various SACs, the applicability of this protocol to classical catalysts featuring metal nanoparticles supported on carbon was investigated. We focused on Pt nanoparticles on carbon (Figure S22) because they are one of the most widely used active materials in electrocatalysis and their SD can be estimated by the conventional voltammetric ECSA measurement methods (i.e., H_{UPD} and CO-stripping). Four commercial Pt catalysts with different particle sizes (ca. 2.5, 2.9, 3.8, and 4.5 nm estimated by transmission electron microscopy; TEM) were introduced to evaluate the precision of the cyanide adsorption method (Figures S23 and S24 and Table S3). The SD variations caused by different sizes of Pt nanoparticles were distinguishable by the ECSA measurements (Figure 4d), which showed a decrease in the ECSA as the particle size increased (at fixed Pt loading). Similar to the voltammetric methods, the spectrophotometry method, in which E_{third} was set to 0.6 V_{RHE} (instead of 1.0 V_{RHE} used for the SACs) to prevent the surface oxide formation of Pt nanoparticles, also successfully differentiated the SDs of the Pt nanoparticle catalysts (Figure 4e). The $\Delta C_{CN^-}^{electrolyte}$ value decreased from 173 to 56 μM with an increase in the particle size, a trend similar to that observed for ECSA.

Despite the non-negligible uncertainty in the SD calculation for the Pt nanoparticles with $\Delta C_{CN^-}^{electrolyte}$, which was caused by the different cyanide adsorption modes depending on the Pt sites,[57] their U values were estimated with an assumption of the coverage (i.e., CN^-/Pt) to be 0.5, based on the previous measurements for a model Pt(111) surface.[58] The calculated U value was 67% for 2.5 nm Pt nanoparticles, which decreased to 56, 41, and 22% with an increase in the particle size to 2.9, 3.8, and 4.5 nm, respectively (Figure 4c,f). This assumption seemingly led to an overestimation of the estimated U values in comparison to those obtained by CO-stripping voltammetry (i.e., $ECSA_{CO}$; U = 53, 39, 21, and 14%, respectively), probably due to the non-negligible contributions of other sites (e.g., Pt(100) or edge) with different adsorption modes of cyanide.[57] However, rough consideration of the different surface coverages of the heterogeneous Pt sites, for instance, CN^-/Pt = 0.5, 1.0, and 1.0 for Pt(111), Pt(100), and edge, respectively[59] (Supplementary Note 4), could alleviate the deviations between the U values obtained with different probe molecules (i.e., cyanide and CO; Figure S25), providing a clue for the precise measurement of the U value of Pt nanoparticles if an accurate coverage of each facet is determined.

Based on the case studies with various SACs and Pt nanoparticles, the precise quantification of SD can be achieved by spectrophotometry using a cyanide probe under electrochemical operating conditions. Then, the TOF values for the $Me_{0.5}NC$ catalysts, Pt/HSC, and Pt nanoparticles in ORR were estimated at 0.80, 0.65, and 0.90 V_{RHE}, respectively (Figure 4g). The intrinsic ORR activity of $Fe_{0.5}NC$ (0.40 ± 0.05 e $site^{-1}$ s^{-1} at 0.80 V_{RHE}) surpassed that of all other $Me_{0.5}NC$ catalysts (0.06 ± 0.03 e $site^{-1}$ s^{-1} at 0.80 V_{RHE}), and in the alkaline medium, the TOF of $Fe_{0.5}NC$ (2.00 ± 0.05 e $site^{-1}$ s^{-1} at 0.80 V_{RHE}) considerably exceeded that obtained in the acidic medium. These results are in good agreement with previous reports on the center metal and pH effects on the ORR catalysis of the Me−N−C catalysts,[60−62] and experimentally demonstrate for the first time that the higher ORR activity of Fe−N−C in comparison to those of other Me−N−C catalysts is due to the higher TOF of $Fe-N_x$ sites, not due to the changes in SD. In Pt/HSC, the full atomic dispersion of Pt (i.e., U = 100%) and its selective two-electron ORR pathway in an acidic medium (Figure S21d) resulted in a low TOF value of 0.80×10^{-2} e $site^{-1}$ s^{-1}, even at a low potential of 0.65 V_{RHE}. The TOF of the 2.5 nm Pt nanoparticle was determined to be 2.08 e $site^{-1}$ s^{-1} at 0.90 V_{RHE}, which decreased to 0.67, 0.26, and 0.13 e $site^{-1}s^{-1}$ with an increase in the particle size to 2.9, 3.8, and 4.5 nm, respectively. These TOF values were slightly lower than those calculated from $ECSA_{CO}$ (2.63, 0.96, 0.51, and 0.20 e $site^{-1}s^{-1}$, respectively) because of the overestimation of the U values with the cyanide probe. However, consideration of the contributions of different heterogeneous Pt sites (i.e., CN^-/Pt = 0.5, 1.0, and 1.0 for Pt(111), Pt(100), and edge, respectively) reduced the deviations between the TOF values determined with the cyanide and CO probes (Figure S25c), and the values were similar to those reported in the literature (10^{-1}−10^0 e $site^{-1}$ s^{-1} estimated by ECSA).[63,64] Therefore, the versatile applicability of this analytical strategy is demonstrated for the SD and TOF quantifications of a series of atomically dispersed transition/noble metal catalysts and Pt nanoparticles in a wide pH range (1−13) of electrolytes.

CONCLUSIONS AND PERSPECTIVES

In summary, the *in situ* SD quantification method provides a new experimental approach to evaluate the key descriptors of catalytic activity, that is, SD and TOF. The introduction of cyanide as an ionic probe and its titration by UV−vis spectrophotometry enabled the determination of these descriptors of the Fe−N−C catalyst over a wide range of electrolyte pH values. In addition, this analytical methodology is widely applicable to a series of atomically dispersed transition/noble metal catalysts and metallic Pt nanoparticles. However, the developed method has an important safety issue owing to the toxic release of $HCN_{(g)}$ in an acidic environment. Extreme caution is needed during the application of this method (please read the Experimental Section carefully before performing the experiments), and it is strongly recommended that the experiments are performed with appropriate safety precautions (e.g., fume hood, HCN gas detector, etc.) or in neutral/alkaline environments. Considering the safety concerns, its scalable generality in SD and TOF evaluations can likely afford a fundamental atomic-level understanding of the electrocatalytic activity, particularly for the SACs (except Fe−N−C), whose trends in site-specific catalytic activity have been evaluated exclusively by density functional theory calculations without direct experimental confirmation.[65−67] Experimental knowledge of the SD and TOF that can be acquired for a broad range of SACs and under various synthesis conditions using this method can provide important insights and ultimately allow the establishment of structure−SD and structure−TOF relationships, allowing the rational development of novel catalysts with improved SD and TOF in the future. Specifically, this method can allow the understanding of the detailed ORR-promoting effect observed via codoping of Me−N−C catalysts with other *p*-block elements (e.g., sulfur) or post-treatment of Me−N−C with final pyrolysis in ammonia.[26,68,69] Currently, it is unclear whether the promoting effect is due to an increased SD or TOF value.[70,71]

https://doi.org/10.1021/jacsau.1c00074
JACS Au 2021, 1, 586−597

EXPERIMENTAL SECTION

Catalyst Preparation

The $Me_{0.5}NC$ catalysts were prepared using Me^{2+} acetate salts (95−98%, Sigma-Aldrich), phen (≥99%, Sigma-Aldrich), and ZIF-8 (Basolite Z1200, BASF). The precursor powders (1 g) containing Me/phen/ZIF-8 with a mass ratio of 0.5/20/80 were placed in a ZrO_2 crucible with 100 ZrO_2 balls (5 mm in diameter) and homogenized using a ball mill with four cycles of 30 min each at 400 rpm. The powder mixture was then pyrolyzed at 1323 K in N_2 for 1 h, and $Me_{0.5}NC$ catalysts were collected after cooling to RT.[20,44,72] The $Me_{0.5}NC$ catalysts contained ca. 1.5 wt % of Me content, as confirmed by inductively coupled plasma-atomic emission spectroscopy (ICP-AES). Recently, simple and general strategies enabling the controlled synthesis of a series of SACs have also been developed.[73,74] For the synthesis of the Fe-free NC catalyst, a precursor mixture comprising phen and ZIF-8 was dry ball-milled and pyrolyzed, similar to the method for $Me_{0.5}NC$. Owing to the presence of trace amounts of Fe impurities in the commercial ZIF-8 (>100 ppm),[75] NC was individually synthesized using Fe-free ZIF-8, which was prepared by mixing 2-methylimidazole (2-MeIm; 99%, Sigma-Aldrich) and Zn nitrate hexahydrate (Zn salt; 98%, Sigma-Aldrich) in an aqueous solution (Zn salt/2-MeIm/water molar ratio of 1/60/2228).[76] Carbon with high sulfur content (HSC) was synthesized by chemical vapor deposition (CVD) of acetylene/H_2S mixed gas (1.4/1.4% in He) on NaX zeolite (5 g) at 823 K for 24 h.[52,53] After CVD, the resulting carbon/zeolite composite was further treated at 1073 K under 5% H_2S/He flow (80 mL min^{-1}) for 3 h. HSC was collected after etching the zeolite template with an aqueous HF/HCl solution (1.1/0.8 wt %). Thereafter, 5 wt % Pt was supported on the HSC by conventional wet impregnation and subsequent H_2 reduction. HSC (0.3 g) and H_2PtCl_6·5·$5H_2O$ (0.04 g; 99%, Kojima Chemicals) were dispersed/dissolved in 100 mL of deionized water, and the solvent was evaporated at 353 K. The resultant powder sample was reduced at 523 K for 3 h under H_2 flow (200 mL min^{-1}). Commercial Pt nanoparticles, HiSPEC 2000 (2.5 nm), HiSPEC 3000 (2.9 nm), HiSPEC 4000 (3.8 nm), and HiSPEC 9000 (4.5 nm), were purchased from Thermo Fisher Scientific.

Physicochemical Characterization

X-ray diffraction (XRD) patterns were obtained using a high-resolution X-ray diffractometer (X'Pert PRO MPD, PANalytical) equipped with a Cu K_α X-ray source at an accelerating voltage of 60 kV and a current of 55 mA with a scan rate of 10° min^{-1} and a step-size of 0.02°. Raman spectra were obtained using an NRS-5000 series Raman spectrometer (JASCO) with 633 nm laser excitation. ICP-AES analysis was carried out using a POLYSCAN 61E system (Hewlett-Packard). X-ray photoelectron spectroscopy (XPS) measurements were performed with a *K*-Alpha$^+$ (Thermo Scientific) instrument equipped with a microfocused monochromator X-ray source. The binding energies were calibrated using the adventitious C_{1s} signal at 284.5 eV as a reference. The XPS data were analyzed using XPSPEAK41 software with a ± 0.1 eV deviation in the binding energy. The XPS-N_{1s} spectra were fitted to four N species: pyridinic-N (398.5 eV), pyrrolic-N (400.1 eV), graphitic-N (401.1 eV), and pyridinic-oxide (403.2 eV).[77] The binding energy used for the peak deconvolution of the XPS-Pt spectra (for $4f_{7/2}$) was 72.2 eV for Pt^{2+} with a spin−orbit splitting of 3.33 eV.[52] XAS measurements were performed with a synchrotron radiation light source in the transmission mode at Pohang Accelerator Laboratory (8C, Nano XAFS). The XAS energy scale was calibrated using each metal foil before the measurements to correct any energy shift during data acquisition. The ^{57}Fe Mössbauer spectrum was acquired using a ^{57}Co source in Rh. The measurement was performed by maintaining both the source and absorber at 5 K. The spectrometer was operated using a triangular velocity waveform, and a NaI scintillation detector was used to detect γ-rays. TEM and high-angle annular dark field scanning transmission electron microscopy (HAADF-STEM) analyses were carried out using a JEM-2100 LaB6 (Jeol) and Titan 80−300 (FEI), respectively.

Electrochemical Characterization

The electrochemical properties were investigated using a VMP3 potentiostat (Bio-Logic) in a three-electrode cell equipped with a graphite rod counter electrode and a saturated Ag/AgCl reference electrode (RE-1A for acidic/neutral media and RE-16 for alkaline medium, EC-Frontier). The reference electrode was doubly separated using glass and polyetheretherketone bridge tubes for acidic/neutral and alkaline media, respectively. The electrolyte was prepared with ultrapure water (>18.2 MΩ, Sartorius) and $HClO_4$ (70%, Sigma-Aldrich), phosphoric acid (≥85%, Sigma-Aldrich), or KOH (99.99%, trace metal basis, Sigma-Aldrich). The reference electrode was calibrated against a Pt electrode in a H_2-saturated electrolyte, and all potentials were reported on a reversible hydrogen electrode (RHE) scale. The $Me_{0.5}NC$ catalyst inks were prepared by dispersing 10 mg of the catalyst in an aqueous solution (3472 μL of deionized water, 267 μL of isopropanol, and 80 μL of 5 wt % Nafion solution). After ultrasonication of the suspension for 30 min, working electrodes were prepared by dropping 15 μL of catalyst ink onto a glassy carbon disk (0.196 cm^2) of the rotating disk electrode (01169, ALS). The catalyst loadings were set to 200 $\mu g\ cm^{-2}$ for $Me_{0.5}NC$ and 20 $\mu g_{Pt}\ cm^{-2}$ for Pt/HSC and Pt nanoparticle catalysts. To prevent (or minimize) any cyanide desorption from the catalytic sites, the ORR polarization curves were recorded by LSV without a typical electrochemical cleaning step (potential cycling in general).[78] The LSV curves were measured from 0.70 V_{RHE} to 1.05 V_{RHE} with a scan rate of 1 mV s^{-1} and a rotation speed of 900 rpm in an O_2-saturated electrolyte. Electrochemical CO-stripping was conducted to determine the $ECSA_{CO}$ values of the Pt nanoparticle catalysts. After CO adsorption at 0.05 V_{RHE} in a CO-saturated electrolyte and subsequent removal of dissolved CO from the electrolyte, two cycles of CV were conducted in the potential range of 0.05−1.2 V_{RHE} at a scan rate of 50 mV s^{-1}.

In situ SD Quantification Method

***Caution**: For safety reasons, the sequence of experiments should be done very carefully when performing the same or similar tests elsewhere. We strongly emphasize that all experiments with cyanide must be conducted in a fume hood or an isolated place such as a glovebox. The researcher(s) must be equipped with an HCN detector during the experiments to avoid any inhalation of HCN. The addition of KCN powder directly to the acid solution is strictly prohibited. Please refer to* Supplementary Note 5 *for detailed information on the laboratory safety guidelines for cyanide.*

In situ SD quantification was performed in a two-compartment electrochemical H-type cell contacted by a Nafion 115 membrane (DuPont), which separated the working electrode from the counter and reference electrodes. Two graphite rods (6.5 mm in diameter) were used as the working and counter electrodes, and the Ag/AgCl electrode was used as the reference electrode. The aqueous cyanide solution was prepared with deaerated ultrapure water and KCN (≥96%, Sigma-Aldrich).

Cyanide poisoning was conducted in an Ar-filled chamber to prevent any undesirable O_2 dissolution in the electrolyte and subsequent competitive adsorption of O_2 on the samples. First, the catalyst powder (30 mg) was dispersed in the electrolyte and mechanically stirred with a magnetic bar at a rotation speed of ca. 300 rpm to prevent sedimentation. Prior to the analysis, predissolved O_2 in the electrolyte was degassed by Ar purging for 30 min at the OCP. Thereafter, with continuous Ar purging and mechanical stirring, a potential of 0.5 V_{RHE} was applied to the working electrode until the measured *j* reached zero (ca. for 20 min), where the catalyst particles collided and electrified during convective motion. After stabilization for 10 min at a specific potential (typically 1.0 V_{RHE}, but 0.6 V_{RHE} for Pt nanoparticles to prevent the formation of surface oxide), aqueous cyanide solution (8 mM) was injected into both compartments, and the initial $C_{CN^-}^{electrolyte}$ value was adjusted to 200 μM. Catalyst poisoning was carried out for 15 min at an identical potential for the stabilization step, and the compartment was fully closed without any gas purging to prevent cyanide loss via the degasification of $HCN_{(aq)}$. The $\Delta C_{CN^-}^{electrolyte}$ value in the filtered electrolyte was measured after dilution with deionized water (electrolyte/water = 1/19 volume ratio). For spectrophotometric titration of $\Delta C_{CN^-}^{electrolyte}$, the diluted electrolyte

https://doi.org/10.1021/jacsau.1c00074
JACS Au 2021, 1, 586−597

(400 μL) was mixed with 30 mM *p*-nitrobenzaldehyde solution (400 μL; ≥95%, TGI), 0.6 mM tetrazolium blue chloride solution (400 μL; Sigma-Aldrich), methanol (760 μL; ≥99.8%, Sigma-Aldrich), and 0.2 M NaOH (40 μL; 99.99%, trace metals basis, Sigma-Aldrich). It is of note that a fixed amount of solution added for titration was not considered in the dilution ratio. Subsequently, the color change to purple was monitored at 520 nm using an UV−vis spectrophotometer (Genesis 400, Thermo-Fisher Scientific) with reference to a blank electrolyte.[46,47] The cyanide-poisoned catalyst filtered after the poisoning protocol was rinsed with deionized water, and its ORR activity was measured to calculate the difference in *j* values between the pristine and poisoned catalysts (i.e., Δ*j*).

■ ASSOCIATED CONTENT

Supporting Information

The Supporting Information is available free of charge at https://pubs.acs.org/doi/10.1021/jacsau.1c00074.

Physicochemical characteristics of $Fe_{0.5}NC$; ORR activity measurement protocol for *in situ* SD quantification using cyanide probe; non-site-specific adsorption of cyanide on Fe−N_x moieties; different cyanide adsorption modes of heterogeneous Pt sites with different surface coverages; spectrophotometric titration results; ORR polarization curves before and after cyanide poisoning; CO chemisorption and NO_2^--stripping results; laboratory safety guidelines (PDF)

■ AUTHOR INFORMATION

Corresponding Authors

Frédéric Jaouen − *ICGM, Universite de Montpellier, CNRS, ENSCM, Montpellier 34095, France;* orcid.org/0000-0001-9836-3261; Email: frederic.jaouen@umontpellier.fr

Chang Hyuck Choi − *School of Materials Science and Engineering, Gwangju Institute of Science and Technology, Gwangju 61005, Republic of Korea;* orcid.org/0000-0002-2231-6116; Email: chchoi@gist.ac.kr

Authors

Geunsu Bae − *School of Materials Science and Engineering, Gwangju Institute of Science and Technology, Gwangju 61005, Republic of Korea*

Haesol Kim − *School of Materials Science and Engineering, Gwangju Institute of Science and Technology, Gwangju 61005, Republic of Korea*

Hansol Choi − *School of Materials Science and Engineering, Gwangju Institute of Science and Technology, Gwangju 61005, Republic of Korea*

Pyeonghwa Jeong − *Department of Chemistry, Duke University, Durham, North Carolina 27708, United States*

Dong Hyun Kim − *School of Materials Science and Engineering, Gwangju Institute of Science and Technology, Gwangju 61005, Republic of Korea*

Han Chang Kwon − *Department of Chemical and Biomolecular Engineering, Korea Advanced Institute of Science and Technology, Daejeon 34141, Republic of Korea*

Kug-Seung Lee − *Beamline Department, Pohang Accelerator Laboratory, Pohang University of Science and Technology, Pohang 37673, Republic of Korea;* orcid.org/0000-0002-7570-8404

Minkee Choi − *Department of Chemical and Biomolecular Engineering, Korea Advanced Institute of Science and Technology, Daejeon 34141, Republic of Korea;* orcid.org/0000-0003-0827-2572

Hyung-Suk Oh − *Clean Energy Research Center, Korea Institute of Science and Technology, Seoul 02792, Republic of Korea; KHU-KIST Department of Conversing Science and Technology, Kyung Hee University, Seoul 02447, Republic of Korea;* orcid.org/0000-0002-0310-6666

Complete contact information is available at: https://pubs.acs.org/10.1021/jacsau.1c00074

Author Contributions

○G.B. and H.K. contributed equally to this work.

Notes

The authors declare no competing financial interest.

■ ACKNOWLEDGMENTS

This work was supported by the National Research Foundation of Korea (NRF) grant funded by the Korea government (MSIT; NRF-2019M3D1A1079309 and 2020R1A2C4002233) and by the Korea Institute of Science and Technology (KIST) institutional program. Experiments at PLS-II were supported in part by MSIT and POSTECH.

■ REFERENCES

(1) Ertl, G. Reactions at Surfaces: From Atoms to Complexity (Nobel Lecture). *Angew. Chem., Int. Ed.* **2008**, *47* (19), 3524−3535.

(2) Schauermann, S.; Nilius, N.; Shaikhutdinov, S.; Freund, H.-J. Nanoparticles for Heterogeneous Catalysis: New Mechanistic Insights. *Acc. Chem. Res.* **2013**, *46* (8), 1673−1681.

(3) Kozuch, S.; Martin, J. M. L. "Turning Over" Definitions in Catalytic Cycles. *ACS Catal.* **2012**, *2* (12), 2787−2794.

(4) Zagal, J. H.; Specchia, S.; Atanassov, P. Mapping Transition Metal-MN_4 Macrocyclic Complex Catalysts Performance for the Critical Reactivity Descriptors. *Curr. Opin. Electrochem.* **2021**, *27*, 100683.

(5) Burcham, L. J.; Briand, L. E.; Wachs, I. E. Quantification of Active Sites for the Determination of Methanol Oxidation Turn-Over Frequencies Using Methanol Chemisorption and In Situ Infrared Techniques. 2. Bulk Metal Oxide Catalysts. *Langmuir* **2001**, *17* (20), 6175−6184.

(6) Li, X.; Wei, S.; Zhang, Z.; Zhang, Y.; Wang, Z.; Su, Q.; Gao, X. Quantification of the Active Site Density and Turnover Frequency for Soot Combustion with O_2 on Cr Doped CeO_2. *Catal. Today* **2011**, *175* (1), 112−116.

(7) Sullivan, M. M.; Held, J. T.; Bhan, A. Structure and Site Evolution of Molybdenum Carbide Catalysts Upon Exposure to Oxygen. *J. Catal.* **2015**, *326*, 82−91.

(8) Bergeret, G.; Gallezot, P. Particle Size and Dispersion Measurements. In *Handbook of Heterogeneous Catalysis*; Ertl, G., Knözinger, H., Schüth, F., Weitkamp, J., Eds.; Wiley-VCH: Weinheim, Germany, 2008; Vol. *1*, pp 738−765.

(9) Goodwin, J. G., Jr.; Kim, S.; Rhodes, W. D. Turnover Frequencies in Metal Catalysis: Meanings, Functionalities and Relationships. In *Catalysis*; Spivey, J. J., Roberts, G. W., Eds.; The Royal Society of Chemistry: London, 2004; Vol. *17*, pp 320−348.

(10) Rudi, S.; Cui, C.; Gan, L.; Strasser, P. Comparative Study of the Electrocatalytically Active Surface Areas (ECSAs) of Pt Alloy Nanoparticles Evaluated by H_{upd} and CO-Stripping Voltammetry. *Electrocatalysis* **2014**, *5* (4), 408−418.

(11) Lorenz, W. J.; Hermann, H. D.; Wüthrich, N.; Hilbert, F. The Formation of Monolayer Metal Films on Electrodes. *J. Electrochem. Soc.* **1974**, *121* (9), 1167.

(12) Herrero, E.; Buller, L. J.; Abruña, H. D. Underpotential Deposition at Single Crystal Surfaces of Au, Pt, Ag and Other Materials. *Chem. Rev.* **2001**, *101* (7), 1897−1930.

(13) Woods, R. Hydrogen Adsorption on Platinum, Iridium and Rhodium Electrodes at Reduced Temperatures and the Determi-

nation of Real Surface Area. *J. Electroanal. Chem. Interfacial Electrochem.* **1974**, *49* (2), 217−226.
(14) Binninger, T.; Fabbri, E.; Kötz, R.; Schmidt, T. J. Determination of the Electrochemically Active Surface Area of Metal-Oxide Supported Platinum Catalyst. *J. Electrochem. Soc.* **2014**, *161* (3), H121−H128.
(15) Brightman, E.; Hinds, G.; O'Malley, R. In Situ Measurement of Active Catalyst Surface Area in Fuel Cell Stacks. *J. Power Sources* **2013**, *242*, 244−254.
(16) Dao, D. V.; Adilbish, G.; Le, T. D.; Lee, I.-H.; Yu, Y.-T. Triple Phase Boundary and Power Density Enhancement in PEMFCs of a Pt/C Electrode with Double Catalyst Layers. *RSC Adv.* **2019**, *9* (27), 15635−15641.
(17) Ou, H.; Wang, D.; Li, Y. How to Select Effective Electrocatalysts: Nano or Single Atom? *Nano Select* **2021**, *2* (3), 492−511.
(18) Proietti, E.; Jaouen, F.; Lefèvre, M.; Larouche, N.; Tian, J.; Herranz, J.; Dodelet, J.-P. Iron-Based Cathode Catalyst with Enhanced Power Density in Polymer Electrolyte Membrane Fuel Cells. *Nat. Commun.* **2011**, *2* (1), 416.
(19) Chung, H. T.; Cullen, D. A.; Higgins, D.; Sneed, B. T.; Holby, E. F.; More, K. L.; Zelenay, P. Direct Atomic-Level Insight into the Active Sites of a High-Performance PGM-Free ORR Catalyst. *Science* **2017**, *357* (6350), 479.
(20) Li, J.; Chen, M.; Cullen, D. A.; Hwang, S.; Wang, M.; Li, B.; Liu, K.; Karakalos, S.; Lucero, M.; Zhang, H.; Lei, C.; Xu, H.; Sterbinsky, G. E.; Feng, Z.; Su, D.; More, K. L.; Wang, G.; Wang, Z.; Wu, G. Atomically Dispersed Manganese Catalysts for Oxygen Reduction in Proton-Exchange Membrane Fuel Cells. *Nat. Catal.* **2018**, *1* (12), 935−945.
(21) Shi, Z.; Yang, W.; Gu, Y.; Liao, T.; Sun, Z. Metal-Nitrogen-Doped Carbon Materials as Highly Efficient Catalysts: Progress and Rational Design. *Adv. Sci.* **2020**, *7* (15), 2001069.
(22) Lei, C.; Wang, Y.; Hou, Y.; Liu, P.; Yang, J.; Zhang, T.; Zhuang, X.; Chen, M.; Yang, B.; Lei, L.; Yuan, C.; Qiu, M.; Feng, X. Efficient Alkaline Hydrogen Evolution on Atomically Dispersed Ni−N_x Species Anchored Porous Carbon with Embedded Ni Nanoparticles by Accelerating Water Dissociation Kinetics. *Energy Environ. Sci.* **2019**, *12* (1), 149−156.
(23) Gu, J.; Hsu, C.-S.; Bai, L.; Chen, H. M.; Hu, X. Atomically Dispersed Fe^{3+} Sites Catalyze Efficient CO_2 Electroreduction to CO. *Science* **2019**, *364* (6445), 1091.
(24) Li, J.; Ghoshal, S.; Liang, W.; Sougrati, M.-T.; Jaouen, F.; Halevi, B.; McKinney, S.; McCool, G.; Ma, C.; Yuan, X.; Ma, Z.-F.; Mukerjee, S.; Jia, Q. Structural and Mechanistic Basis for the High Activity of Fe−N−C Catalysts toward Oxygen Reduction. *Energy Environ. Sci.* **2016**, *9* (7), 2418−2432.
(25) Jia, Q.; Ramaswamy, N.; Tylus, U.; Strickland, K.; Li, J.; Serov, A.; Artyushkova, K.; Atanassov, P.; Anibal, J.; Gumeci, C.; Barton, S. C.; Sougrati, M.-T.; Jaouen, F.; Halevi, B.; Mukerjee, S. Spectroscopic Insights into the Nature of Active Sites in Iron−Nitrogen−Carbon Electrocatalysts for Oxygen Reduction in Acid. *Nano Energy* **2016**, *29*, 65−82.
(26) Luo, F.; Roy, A.; Silvioli, L.; Cullen, D. A.; Zitolo, A.; Sougrati, M. T.; Oguz, I. C.; Mineva, T.; Teschner, D.; Wagner, S.; Wen, J.; Dionigi, F.; Kramm, U. I.; Rossmeisl, J.; Jaouen, F.; Strasser, P. *P*-Block Single-Metal-Site Tin/Nitrogen-Doped Carbon Fuel Cell Cathode Catalyst for Oxygen Reduction Reaction. *Nat. Mater.* **2020**, *19*, 1215−1223.
(27) Li, J.; Sougrati, M. T.; Zitolo, A.; Ablett, J. M.; Oğuz, I. C.; Mineva, T.; Matanovic, I.; Atanassov, P.; Huang, Y.; Zenyuk, I.; Di Cicco, A.; Kumar, K.; Dubau, L.; Maillard, F.; Dražić, G.; Jaouen, F. Identification of Durable and Non-Durable FeN_x Sites in Fe−N−C Materials for Proton Exchange Membrane Fuel Cells. *Nat. Catal.* **2021**, *4* (1), 10−19.
(28) Sato, S.; Namba, K.; Hara, K.; Fukuoka, A.; Murakoshi, K.; Uosaki, K.; Ikeda, K. Kinetic Behavior of Catalytic Active Sites Connected with a Conducting Surface through Various Electronic Coupling. *J. Phys. Chem. C* **2016**, *120* (4), 2159−2165.
(29) Toyama, T.; Sato, S.; Motobayashi, K.; Uosaki, K.; Ikeda, K. A Rotating Disk Electrode Study on Catalytic Activity of Iron(II) Phthalocyanine-Modified Electrodes for Oxygen Reduction in Acidic Media. *J. Solid State Electrochem.* **2021**, *25* (1), 141−147.
(30) Sahraie, N. R.; Kramm, U. I.; Steinberg, J.; Zhang, Y.; Thomas, A.; Reier, T.; Paraknowitsch, J.-P.; Strasser, P. Quantifying the Density and Utilization of Active Sites in Non-Precious Metal Oxygen Electroreduction Catalysts. *Nat. Commun.* **2015**, *6* (1), 8618.
(31) Malko, D.; Kucernak, A.; Lopes, T. *In Situ* Electrochemical Quantification of Active Sites in Fe−N/C Non-Precious Metal Catalysts. *Nat. Commun.* **2016**, *7* (1), 13285.
(32) Ju, W.; Bagger, A.; Hao, G.-P.; Varela, A. S.; Sinev, I.; Bon, V.; Roldan Cuenya, B.; Kaskel, S.; Rossmeisl, J.; Strasser, P. Understanding Activity and Selectivity of Metal-Nitrogen-Doped Carbon Catalysts for Electrochemical Reduction of CO_2. *Nat. Commun.* **2017**, *8* (1), 944.
(33) Luo, F.; Choi, C. H.; Primbs, M. J. M.; Ju, W.; Li, S.; Leonard, N. D.; Thomas, A.; Jaouen, F.; Strasser, P. Accurate Evaluation of Active-Site Density (SD) and Turnover Frequency (TOF) of PGM-Free Metal−Nitrogen-Doped Carbon (MNC) Electrocatalysts using CO cryo Adsorption. *ACS Catal.* **2019**, *9* (6), 4841−4852.
(34) Rosca, V.; Duca, M.; de Groot, M. T.; Koper, M. T. M. Nitrogen Cycle Electrocatalysis. *Chem. Rev.* **2009**, *109* (6), 2209−2244.
(35) Einsle, O.; Messerschmidt, A.; Huber, R.; Kroneck, P. M. H.; Neese, F. Mechanism of the Six-Electron Reduction of Nitrite to Ammonia by Cytochrome *c* Nitrite Reductase. *J. Am. Chem. Soc.* **2002**, *124* (39), 11737−11745.
(36) de Groot, M. T.; Merkx, M.; Koper, M. T. M. Heme Release in Myoglobin−DDAB Films and Its Role in Electrochemical NO Reduction. *J. Am. Chem. Soc.* **2005**, *127* (46), 16224−16232.
(37) de Groot, M. T.; Merkx, M.; Wonders, A. H.; Koper, M. T. M. Electrochemical Reduction of NO by Hemin Adsorbed at Pyrolitic Graphite. *J. Am. Chem. Soc.* **2005**, *127* (20), 7579−7586.
(38) de Groot, M. T.; Merkx, M.; Koper, M. T. M. Bioinspired Electrocatalytic Reduction of Nitric Oxide by Immobilized Heme Groups. *C. R. Chim.* **2007**, *10* (4), 414−420.
(39) Primbs, M.; Sun, Y.; Roy, A.; Malko, D.; Mehmood, A.; Sougrati, M.-T.; Blanchard, P.-Y.; Granozzi, G.; Kosmala, T.; Daniel, G.; Atanassov, P.; Sharman, J.; Durante, C.; Kucernak, A.; Jones, D.; Jaouen, F.; Strasser, P. Establishing Reactivity Descriptors for Platinum Group Metal (PGM)-Free Fe−N−C Catalysts for PEM Fuel Cells. *Energy Environ. Sci.* **2020**, *13* (8), 2480−2500.
(40) Li, Y.; Zhou, W.; Wang, H.; Xie, L.; Liang, Y.; Wei, F.; Idrobo, J.-C.; Pennycook, S. J.; Dai, H. An Oxygen Reduction Electrocatalyst Based on Carbon Nanotube−Graphene Complexes. *Nat. Nanotechnol.* **2012**, *7* (6), 394−400.
(41) Tylus, U.; Jia, Q.; Strickland, K.; Ramaswamy, N.; Serov, A.; Atanassov, P.; Mukerjee, S. Elucidating Oxygen Reduction Active Sites in Pyrolyzed Metal−Nitrogen Coordinated Non-Precious-Metal Electrocatalyst Systems. *J. Phys. Chem. C* **2014**, *118* (17), 8999−9008.
(42) Chung, M. W.; Chon, G.; Kim, H.; Jaouen, F.; Choi, C. H. Electrochemical Evidence for Two Sub-Families of FeN_xC_y Moieties with Concentration-Dependent Cyanide Poisoning. *ChemElectroChem* **2018**, *5* (14), 1880−1885.
(43) Choi, C. H.; Lim, H.-K.; Chung, M. W.; Chon, G.; Ranjbar Sahraie, N.; Altin, A.; Sougrati, M.-T.; Stievano, L.; Oh, H. S.; Park, E. S.; Luo, F.; Strasser, P.; Dražić, G.; Mayrhofer, K. J. J.; Kim, H.; Jaouen, F. The Achilles' Heel of Iron-Based Catalysts During Oxygen Reduction in an Acidic Medium. *Energy Environ. Sci.* **2018**, *11* (11), 3176−3182.
(44) Zitolo, A.; Goellner, V.; Armel, V.; Sougrati, M.-T.; Mineva, T.; Stievano, L.; Fonda, E.; Jaouen, F. Identification of Catalytic Sites for Oxygen Reduction in Iron- and Nitrogen-Doped Graphene Materials. *Nat. Mater.* **2015**, *14* (9), 937−942.
(45) Gupta, S.; Fierro, C.; Yeager, E. The Effects of Cyanide on the Electrochemical Properties of Transition Metal Macrocycles for Oxygen Reduction in Alkaline Solutions. *J. Electroanal. Chem. Interfacial Electrochem.* **1991**, *306* (1), 239−250.

https://doi.org/10.1021/jacsau.1c00074
JACS Au 2021, 1, 586−597

(46) Pitschmann, V.; Kobliha, Z.; Tušarová, I. A Simple Spectrophotometric Determination of Cyanides by *p*-Nitrobenzaldehyde and Tetrazolium Blue. *Adv. Mil. Technol.* **2011**, *6*, 19−27.
(47) Guilbault, G. G.; Kramer, D. N. Ultra Sensitive, Specific Method for Cyanide Using *p*-Nitrobenzaldehyde and *o*-Dinitrobenzene. *Anal. Chem.* **1966**, *38* (7), 834−836.
(48) Kumar, R.; Saha, S.; Dhaka, S.; Kurade, M. B.; Kang, C. U.; Baek, S. H.; Jeon, B.-H. Remediation of Cyanide-Contaminated Environments Through Microbes and Plants: A Review of Current Knowledge and Future Perspectives. *Geosyst. Eng.* **2017**, *20* (1), 28−40.
(49) Yoshikawa, S.; O'Keeffe, D. H.; Caughey, W. S. Investigations of Cyanide as an Infrared Probe of Hemeprotein Ligand Binding Sites. *J. Biol. Chem.* **1985**, *260* (6), 3518−3528.
(50) Sun, Y.; Silvioli, L.; Sahraie, N. R.; Ju, W.; Li, J.; Zitolo, A.; Li, S.; Bagger, A.; Arnarson, L.; Wang, X.; Moeller, T.; Bernsmeier, D.; Rossmeisl, J.; Jaouen, F.; Strasser, P. Activity−Selectivity Trends in the Electrochemical Production of Hydrogen Peroxide over Single-Site Metal−Nitrogen−Carbon Catalysts. *J. Am. Chem. Soc.* **2019**, *141* (31), 12372−12381.
(51) Li, J.; Pršlja, P.; Shinagawa, T.; Martín Fernández, A. J.; Krumeich, F.; Artyushkova, K.; Atanassov, P.; Zitolo, A.; Zhou, Y.; García-Muelas, R.; López, N.; Pérez-Ramírez, J.; Jaouen, F. Volcano Trend in Electrocatalytic CO_2 Reduction Activity over Atomically Dispersed Metal Sites on Nitrogen-Doped Carbon. *ACS Catal.* **2019**, *9* (11), 10426−10439.
(52) Choi, C. H.; Kim, M.; Kwon, H. C.; Cho, S. J.; Yun, S.; Kim, H.-T.; Mayrhofer, K. J. J.; Kim, H.; Choi, M. Tuning Selectivity of Electrochemical Reactions by Atomically Dispersed Platinum Catalyst. *Nat. Commun.* **2016**, *7* (1), 10922.
(53) Kwon, H. C.; Kim, M.; Grote, J.-P.; Cho, S. J.; Chung, M. W.; Kim, H.; Won, D. H.; Zeradjanin, A. R.; Mayrhofer, K. J. J.; Choi, M.; Kim, H.; Choi, C. H. Carbon Monoxide as a Promoter of Atomically Dispersed Platinum Catalyst in Electrochemical Hydrogen Evolution Reaction. *J. Am. Chem. Soc.* **2018**, *140* (47), 16198−16205.
(54) Zhang, J.; Zhao, Y.; Guo, X.; Chen, C.; Dong, C.-L.; Liu, R.-S.; Han, C.-P.; Li, Y.; Gogotsi, Y.; Wang, G. Single Platinum Atoms Immobilized on an MXene as an Efficient Catalyst for the Hydrogen Evolution Reaction. *Nat. Catal.* **2018**, *1* (12), 985−992.
(55) Liu, J.; Jiao, M.; Lu, L.; Barkholtz, H. M.; Li, Y.; Wang, Y.; Jiang, L.; Wu, Z.; Liu, D.-j.; Zhuang, L.; Ma, C.; Zeng, J.; Zhang, B.; Su, D.; Song, P.; Xing, W.; Xu, W.; Wang, Y.; Jiang, Z.; Sun, G. High Performance Platinum Single Atom Electrocatalyst for Oxygen Reduction Reaction. *Nat. Commun.* **2017**, *8* (1), 15938.
(56) Cheng, N.; Stambula, S.; Wang, D.; Banis, M. N.; Liu, J.; Riese, A.; Xiao, B.; Li, R.; Sham, T.-K.; Liu, L.-M.; Botton, G. A.; Sun, X. Platinum Single-Atom and Cluster Catalysis of the Hydrogen Evolution Reaction. *Nat. Commun.* **2016**, *7* (1), 13638.
(57) Ren, B.; Wu, D.-Y.; Mao, B.-W.; Tian, Z.-Q. Surface-Enhanced Raman Study of Cyanide Adsorption at the Platinum Surface. *J. Phys. Chem. B* **2003**, *107* (12), 2752−2758.
(58) Stuhlmann, C.; Villegas, I.; Weaver, M. J. Scanning Tunneling Microscopy and Infrared Spectroscopy as Combined In Situ Probes of Electrochemical Adlayer Structure. Cyanide on Pt(111). *Chem. Phys. Lett.* **1994**, *219* (3), 319−324.
(59) Shao, M.; Peles, A.; Shoemaker, K. Electrocatalysis on Platinum Nanoparticles: Particle Size Effect on Oxygen Reduction Reaction Activity. *Nano Lett.* **2011**, *11* (9), 3714−3719.
(60) Merzougui, B.; Hachimi, A.; Akinpelu, A.; Bukola, S.; Shao, M. A Pt-Free Catalyst for Oxygen Reduction Reaction Based on Fe−N Multiwalled Carbon Nanotube Composites. *Electrochim. Acta* **2013**, *107*, 126−132.
(61) Sgarbi, R.; Kumar, K.; Jaouen, F.; Zitolo, A.; Ticianelli, E. A.; Maillard, F. Oxygen Reduction Reaction Mechanism and Kinetics on M-N_xC_y and M@N-C Active Sites Present in Model M-N-C Catalysts under Alkaline and Acidic Conditions. *J. Solid State Electrochem.* **2021**, *25* (1), 45−56.
(62) Meng, H.; Jaouen, F.; Proietti, E.; Lefèvre, M.; Dodelet, J.-P. pH-Effect on Oxygen Reduction Activity of Fe-Based Electrocatalysts. *Electrochem. Commun.* **2009**, *11* (10), 1986−1989.
(63) Chen, D.; Li, Y.; Liao, S.; Su, D.; Song, H.; Li, Y.; Yang, L.; Li, C. Ultra-High-Performance Core−Shell Structured Ru@Pt/C Catalyst Prepared by a Facile Pulse Electrochemical Deposition Method. *Sci. Rep.* **2015**, *5* (1), 11604.
(64) Jaouen, F.; Jones, D.; Coutard, N.; Artero, V.; Strasser, P.; Kucernak, A. Toward Platinum Group Metal-Free Catalysts for Hydrogen/Air Proton-Exchange Membrane Fuel Cells. *Johnson Matthey Technol. Rev.* **2018**, *62* (2), 231−255.
(65) Patel, A. M.; Ringe, S.; Siahrostami, S.; Bajdich, M.; Nørskov, J. K.; Kulkarni, A. R. Theoretical Approaches to Describing the Oxygen Reduction Reaction Activity of Single-Atom Catalysts. *J. Phys. Chem. C* **2018**, *122* (51), 29307−29318.
(66) Vijay, S.; Gauthier, J. A.; Heenen, H. H.; Bukas, V. J.; Kristoffersen, H. H.; Chan, K. Dipole-Field Interactions Determine the CO_2 Reduction Activity of 2D Fe−N−C Single-Atom Catalysts. *ACS Catal.* **2020**, *10* (14), 7826−7835.
(67) Yao, M.; Shi, Z.; Zhang, P.; Ong, W.-J.; Jiang, J.; Ching, W.-Y.; Li, N. Density Functional Theory Study of Single Metal Atoms Embedded into MBene for Electrocatalytic Conversion of N_2 to NH_3. *ACS Appl. Nano Mater.* **2020**, *3* (10), 9870−9879.
(68) Wang, Y.-C.; Lai, Y.-J.; Song, L.; Zhou, Z.-Y.; Liu, J.-G.; Wang, Q.; Yang, X.-D.; Chen, C.; Shi, W.; Zheng, Y.-P.; Rauf, M.; Sun, S.-G. S-Doping of an Fe/N/C ORR Catalyst for Polymer Electrolyte Membrane Fuel Cells with High Power Density. *Angew. Chem., Int. Ed.* **2015**, *54* (34), 9907−9910.
(69) Hou, Y.; Qiu, M.; Kim, M. G.; Liu, P.; Nam, G.; Zhang, T.; Zhuang, X.; Yang, B.; Cho, J.; Chen, M.; Yuan, C.; Lei, L.; Feng, X. Atomically Dispersed Nickel−Nitrogen−Sulfur Species Anchored on Porous Carbon Nanosheets for Efficient Water Oxidation. *Nat. Commun.* **2019**, *10* (1), 1392.
(70) Ferrandon, M.; Kropf, A. J.; Myers, D. J.; Artyushkova, K.; Kramm, U.; Bogdanoff, P.; Wu, G.; Johnston, C. M.; Zelenay, P. Multitechnique Characterization of a Polyaniline−Iron−Carbon Oxygen Reduction Catalyst. *J. Phys. Chem. C* **2012**, *116* (30), 16001−16013.
(71) Ramaswamy, N.; Tylus, U.; Jia, Q.; Mukerjee, S. Activity Descriptor Identification for Oxygen Reduction on Nonprecious Electrocatalysts: Linking Surface Science to Coordination Chemistry. *J. Am. Chem. Soc.* **2013**, *135* (41), 15443−15449.
(72) Zitolo, A.; Ranjbar-Sahraie, N.; Mineva, T.; Li, J.; Jia, Q.; Stamatin, S.; Harrington, G. F.; Lyth, S. M.; Krtil, P.; Mukerjee, S.; Fonda, E.; Jaouen, F. Identification of Catalytic Sites in Cobalt-Nitrogen-Carbon Materials for the Oxygen Reduction Reaction. *Nat. Commun.* **2017**, *8* (1), 957.
(73) Yin, P.; Yao, T.; Wu, Y.; Zheng, L.; Lin, Y.; Liu, W.; Ju, H.; Zhu, J.; Hong, X.; Deng, Z.; Zhou, G.; Wei, S.; Li, Y. Single Cobalt Atoms with Precise N-Coordination as Superior Oxygen Reduction Reaction Catalysts. *Angew. Chem., Int. Ed.* **2016**, *55* (36), 10800−10805.
(74) Wei, H.; Huang, K.; Zhang, L.; Ge, B.; Wang, D.; Lang, J.; Ma, J.; Wang, D.; Zhang, S.; Li, Q.; Zhang, R.; Hussain, N.; Lei, M.; Liu, L.-M.; Wu, H. Ice Melting to Release Reactants in Solution Syntheses. *Angew. Chem., Int. Ed.* **2018**, *57* (13), 3354−3359.
(75) Zhang, G.; Chenitz, R.; Lefèvre, M.; Sun, S.; Dodelet, J.-P. Is Iron Involved in the Lack of Stability of Fe/N/C Electrocatalysts Used to Reduce Oxygen at the Cathode of PEM Fuel Cells? *Nano Energy* **2016**, *29*, 111−125.
(76) Kida, K.; Okita, M.; Fujita, K.; Tanaka, S.; Miyake, Y. Formation of High Crystalline ZIF-8 in an Aqueous Solution. *CrystEngComm* **2013**, *15* (9), 1794−1801.
(77) Guo, D.; Shibuya, R.; Akiba, C.; Saji, S.; Kondo, T.; Nakamura, J. Active Sites of Nitrogen-Doped Carbon Materials for Oxygen Reduction Reaction Clarified Using Model Catalysts. *Science* **2016**, *351* (6271), 361.
(78) Kocha, S. S.; Shinozaki, K.; Zack, J. W.; Myers, D. J.; Kariuki, N. N.; Nowicki, T.; Stamenkovic, V.; Kang, Y.; Li, D.; Papageorgopoulos, D. Best Practices and Testing Protocols for

https://doi.org/10.1021/jacsau.1c00074
JACS Au 2021, 1, 586−597

Benchmarking ORR Activities of Fuel Cell Electrocatalysts Using Rotating Disk Electrode. *Electrocatalysis* **2017**, *8* (4), 366−374.

https://doi.org/10.1021/jacsau.1c00074
JACS Au 2021, 1, 586−597